J Mar Sci Technol (2008) 13:207–222
DOI 10.1007/s00773-008-0027-0

ORIGINAL ARTICLE

Mathematical model of single-propeller twin-rudder ship

Donghoon Kang · Vishwanath Nagarajan · Kazuhiko Hasegawa · Masaaki Sano

Received: 17 August 2007 / Accepted: 18 June 2008 / Published online: 6 August 2008

Abstract A mathematical model of a single-propeller twin-rudder ship has been developed from captive and free running model experiments. An open water rudder experiment was carried out to figure out the characteristics of the rudder. Captive experiments in a towing tank were carried out to figure out the performance of a single-propeller twin-rudder system on a large vessel. Interactions between the hull, propeller and twin rudders, including mutual interactions between the twin rudders, were expressed with several coefficients that were calculated from the experimental results at various ship speeds. In the analysis, the unique characteristics of a single-propeller twin-rudder ship, which affects rudder forces, were explained and formulated in the mathematical model. The captive model tests were conducted with zero ship's yaw rate, so the interaction coefficients, which are influenced by the yaw rate, are determined from free running model experiments. Validation of the mathematical model of a single-propeller twin-rudder system for a blunt body ship is carried out with an independent set of free running experiments, which were not used for determining the interaction coefficients. The validated numerical model is used for carrying out simulations. Based on simulation results, some recommendations have been proposed for installing a single-propeller twin-rudder system.

Keywords Single-propeller twin-rudder system · Numerical simulation · Maneuverability · Mutual interaction of twin rudders

List of symbols

a_H	interaction force coefficient induced on ship hull by rudder normal force
A_R	rudder area
B	ship breadth
C_b	block coefficient
C_N	rudder normal force coefficient
C_1, C_2, C_3	coefficients of polynomial representing propeller open water thrust characteristics
d	ship draft
D_P	propeller diameter
f_{RS}, f_{RP}	decrement ratio of inflow velocity for starboard and port rudder
F_{NS}, F_{NP}	rudder normal force for starboard and port rudder
F_{NSM}, F_{NPM}	measured rudder normal force in experiment for starboard and port rudder
h_R	rudder height
I_{zz}	yaw moment of inertia
J	real propeller advance ratio
J_s	apparent propeller advance ratio
J_{zz}	added yaw moment of inertia
K_T	propeller thrust coefficient
k_x	coefficient indicating the rate of rudder inflow acceleration due to the propeller
L	ship length

D. Kang
IIHR-Hydroscience and Engineering, College of Engineering, The University of Iowa, Iowa city, IA, USA

V. Nagarajan (✉) · K. Hasegawa
Department of Naval Architecture and Ocean Engineering, Graduate School of Engineering, Osaka University, 2-1 Yamadaoka, Suita, Osaka 565-0871, Japan
e-mail: Vishwanath@naoe.eng.osaka-u.ac.jp

M. Sano
Department of Social and Environmental Engineering, Graduate School of Engineering, Hiroshima University, Higashi-Hiroshima, Hiroshima, Japan

l_{RS}, l_{RP}	flow straightening coefficient of yaw rate for starboard and port rudder
m	ship mass
m_x	added mass in surge
m_y	added mass in sway
n	propeller revolution
r	yaw rate of ship
$R(u)$	ship resistance
s	propeller slip ratio
S_W	ship's wetted surface area
T_M	measured propeller thrust in experiment
t_{P0}	thrust deduction factor in straight running
t_P	thrust deduction factor in maneuvering
t_R	coefficient for deduction of rudder drag
u	surge velocity
$U = \sqrt{u^2 + v^2}$	ship velocity
u_{RS}, u_{RP}	inflow velocity in surge direction to starboard and port rudder
u_{RSM}, u_{RPM}	rudder inflow velocity calculated with measured rudder force for starboard and port rudder
u_{RSP}, u_{RPP}	rudder inflow velocity due to propeller for starboard and port rudder
v	sway velocity
v_{RS}, v_{RP}	inflow velocity in sway direction to starboard and port rudder
x_G	location of center of gravity of ship in x-axis direction
x_H	location of acting point of interaction force induced on ship hull by rudder normal force
x_P	location of propeller in x-axis direction
x_R	location of rudder in x-axis direction
x_t	location of center of gravity of ship's added mass in x-axis direction
X_M	measured force in x-axis direction during captive model test
w_{P0}	effective propeller wake fraction in straight running
w_P	effective propeller wake fraction in maneuvering
w_{RS}, w_{RP}	effective wake fraction for starboard and port rudder
α_{RS}, α_{RP}	effective rudder inflow angle of starboard and port rudder
β	drift angle of ship
δ_S, δ_P	angle of starboard and port rudder
δ_{S0}, δ_{P0}	hydrodynamic neutral angle of starboard and port rudder
δ_{SP}, δ_{PS}	variation of inflow rudder angle due to interaction between starboard and port rudder
ε_S, ε_P	ratio of effective wake fraction in way of propeller and rudder
ρ	water density
γ_{RS}, γ_{RP}	flow straightening coefficient of sway velocity for starboard and port rudder

1 Introduction

Number of ships constructed every year is continuously increasing due to an increase in shipping trade. This has resulted in crowded waterways and a consequent need for increasing ship maneuverability. Efforts in various directions are being made for increasing ship maneuverability. One of the methods of increasing the ship maneuvering performance is by improving its rudder system. A new type of single-propeller twin-rudder system, the VecTwin rudder [1] was introduced for small vessels for this purpose. One of the variants of VecTwin rudder, the Super VecTwin rudder, is reputed to have good maneuvering and propulsion performance in small and medium sized vessels. This rudder type was further developed for large vessels like the VLCC (very large crude carrier), and this variant is called the mariner-type Super VecTwin rudder, hereinafter MSV rudder. Hasegawa et al. [2] investigated the suitability of the MSV rudder for a VLCC model and also compared its maneuvering performance with a mariner rudder by conducting free running experiments. It was shown that since the MSV rudder is behind a single propeller, the inflow speed around each one of the MSV rudders is asymmetric, and this aspect needs to be considered for its installation, and it was concluded that the MSV rudder is suitable for large vessels like VLCCs. Therefore, there is a need to analyze in detail the performance and characteristics of a single-propeller twin-rudder system for different types of vessels. For this purpose, a mathematical model of single-propeller twin-rudder ship needs to be developed.

One of the methods of developing ship's mathematical model is by using the MMG concept [3]. The MMG model was originally developed for a single-propeller, single-rudder system. Some researchers have extended it to a twin-propeller twin-rudder system. Lee et al. [4, 5] developed a mathematical model of twin-propeller twin-rudder system using experiment results. Yoshimura et al. [6] investigated the maneuvering characteristics of different types of twin-propeller twin-rudder ships in deep and shallow water. It was shown that the mechanism of shallow water effect on rudder force is quite different from that on hull damping force, and in shallow water a ship's turning ability can be improved by increasing a ship's propulsive efficiency. A mathematical model of a twin-propeller twin-rudder system for deep and shallow water was also

developed. Kobayashi et al. [7] developed a mathematical model of a twin-propeller twin-rudder ship at cruising speed and low speed maneuvering range and validated it with free running model experiments. Different parameters included in the mathematical model for maneuvering motions were investigated experimentally and a new mathematical model for a twin-propeller twin-rudder ship was proposed. Yumuro [8] investigated a twin-propeller single-rudder system in the absence of a ship hull and proposed a method to determine effective inflow velocity to rudder and rudder normal force. Hamamoto et al. [9] extended the MMG model to a single-propeller twin-rudder ship. Wind tunnel experiments were carried out with a single propeller and twin rudders without the ship hull and forces acting on the twin rudders were measured. From wind tunnel experiment results, mutual interactions between the twin rudders were observed. A practical formula to estimate the lift force of each one of the twin rudders, considering their mutual interactions, was developed based on a theoretical analysis of experiment data. Free running tests of a PCC model ship with a twin-rudder system were also carried out to evaluate its maneuvering performance.

However, the interactions between the hull, a single propeller and twin rudders have not yet been investigated and incorporated in the mathematical model of a single-propeller twin-rudder ship. These are determined and shown in this paper. Open water experiments for a twin rudder were carried out in circulating water channel. Experiments were carried out in towing tank with a model ship installed with a single-propeller twin-rudder system and different characteristics of the rudder inflow velocity and mutual interaction between twin rudders is observed as compared to both single-propeller single-rudder and twin-propeller twin-rudder system. These characteristics are explained and incorporated in the mathematical model and based on them recommendation for installing the single-propeller twin-rudder system has also been proposed. The developed model is validated with free running experiments.

2 Models of the ship and rudder

A VLCC model ship was chosen for the experiments and its particulars are shown in Table 1. The MSV rudder is fitted with a horizontal fin for improving ship's propulsion ability [2]. The horizontal fin is not expected to significantly contribute to the normal force characteristics of the MSV rudder. In this study, for all the experiments the horizontal fin of the MSV rudder was trimmed off. The term "mariner-type VecTwin rudder (hereinafter MVT rudder)" is used for a MSV rudder without a horizontal fin. In this paper, the single-propeller MVT rudder system will be referred as a twin-rudder system, while the single-propeller mariner rudder system will be referred as a single-rudder system. Each one of the twin rudders is a semi-spade rudder with a rudder horn, and the cross section of each twin rudder is similar to that of a Schilling rudder. Therefore, the twin-rudder system has higher normal force coefficient as compared to the mariner rudder. The twin-rudder system studied in this paper is shown in Fig. 1. Main dimensions of the twin rudders are shown in Table 2. Only one of the twin rudders was used for rudder open water experiments and the same twin-rudder was installed on the ship during the experiments in the towing tank. The conditions of the different experiments conducted in the towing tank are summarized in Table 3. During all the experiments in the towing tank the ship's yaw rate is kept zero.

3 Equations of motion

The typical MMG model representation for a maneuvering ship is shown in Eq. 1. Since the experiments in the towing tank were carried out in steady conditions with zero yaw rate, terms on left-hand side of Eq. 1 becomes zero, while the terms on right-hand side of Eq. 1 can be estimated from the measurements of the sensors fitted on the model ship.

$$\left.\begin{aligned}
&(m+m_x)\cdot\dot{u}-m\cdot\left(v\cdot r+x_G\cdot r^2\right)=X_H+X_P+X_R\\
&\left(m+m_y\right)\cdot\dot{v}+\left(m\cdot x_G+m_y\cdot x_t\right)\cdot\dot{r}+m\cdot u\cdot r=Y_H+Y_R\\
&\left(I_{zz}+m\cdot x_G^2+J_{zz}+m_y\cdot x_t^2\right)\cdot\dot{r}+\left(m\cdot x_G+m_y\cdot x_t\right)\cdot\dot{v}\\
&\quad+m\cdot x_G\cdot u\cdot r=N_H+N_R
\end{aligned}\right\}\tag{1}$$

Table 1 Principal dimensions of the model ship

L (m)	4.00	X_G (m)	0.123
B (m)	0.667	S_W (m^2)	4.049
d (m)	0.240	D_P (m)	0.12057
C_b	0.817	P/D_P	0.6669

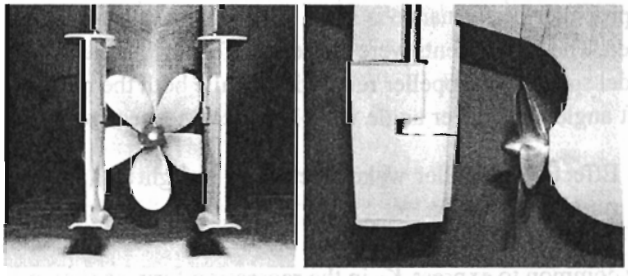

Fig. 1 Layout of a single-propeller twin-rudder system

Table 2 Main dimensions of twin rudders

Particulars		Remark
Height of rudder (m)	0.116	
Breadth of rudder (m)	0.081/0.0565	Top/bottom
A_R (m^2)	0.00672	Effective rudder area
A_R/Ld	1/71.0	
Distance between twin rudders'(m)	0.08	Measured between stock centerline

Table 3 Details of experiment conditions

Experiment		Condition		
Propeller performance tests		$0.1211 \le J_S \le 1.1848$	$\delta_{S_P} = 0°$	$\beta = 0°$
Rudder performance tests	For interaction of ship and rudders	$0.0 \le J_S \le 0.9479$	Various δ_{S_P}	$\beta = 0°$
	For rudder model		$\begin{pmatrix}-30°\\-60°\end{pmatrix} \le \delta_{S_P} \le \begin{pmatrix}60°\\30°\end{pmatrix}$	$\beta = 0°$
	With drift angle	$U = 0.41$ m/s, $n = 7.0$ rps	$\begin{pmatrix}-30°\\-40°\end{pmatrix} \le \delta_{S_P} \le \begin{pmatrix}40°\\30°\end{pmatrix}$	$-20° \le \beta \le 20°$

The experiments were analyzed based on the above MMG model and the interaction coefficients were determined by least square method. The interactions between hull, propeller and twin rudders are expressed with a set of coefficients that are already explained in previous research [2] and some coefficients were added based on physical sense to increase accuracy of the mathematical model of the twin rudders. Due to the geometric restriction, the load cell could be fitted on the stock of only one of the twin rudders at a time. To measure twin-rudder force, each set of experiment is repeated by fitting the load cell alternately on the stock of starboard and port twin rudder, respectively. The coordinate system and various parameters are shown in Fig. 2.

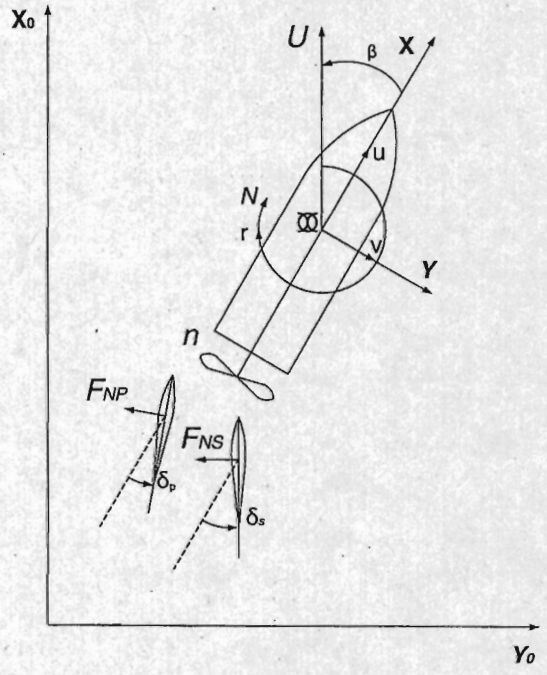

Fig. 2 Coordinate system

4 Mathematical model of the propeller

The analysis of propeller performance is carried out as per the ITTC method [10]. It is assumed that the performance of a propeller with either a twin-rudder or a single-rudder system is similar. This is because, since the propeller is ahead of the rudder, it is assumed that the effect of the rudder on propeller performance is small while the ship has ahead speed. The experiments were carried out for various cases of model speed and propeller revolution, while both the model drift angle and rudder angle were kept zero, respectively.

4.1 Effective propeller wake fraction in straight running condition

It is common to express K_T in the regression form as shown in Eq. 2.

$$\left.\begin{aligned} K_T &= C_1 + C_2 J + C_3 J^2 \\ J &= u(1 - w_P)/(nD_P) \end{aligned}\right\} \quad (2)$$

The thrust coefficient K_T is estimated from the measured propeller thrust T_M using Eq. 3. With K_T as input data, J is estimated using Eq. 2. For ship's straight running condition, w_{P0} is estimated using Eq. 4 and its values are shown in Fig. 3.

$$K_T = T_M/\rho n^2 D_P^4 \tag{3}$$

$$1 - w_{P0} = \frac{JD_P n}{u} \tag{4}$$

For the mariner rudder, it is common to express $1 - w_{P0}$ as a quadratic function of J_S [11]. Similarly, for a twin-rudder system a quadratic function of J_S as shown in Eq. 5 is assumed for formulating $1 - w_{P0}$.

$$\left.\begin{aligned} 1 - w_{P0} &= a_1 + a_2 J_S + a_3 J_S^2 \\ J_S &= {}^{u}/_{(nD_P)} \end{aligned}\right\} \tag{5}$$

A regression line of w_{P0} against C_b for different ships estimated from full-scale trial data is provided by Lewis [12]. From this line, w_{P0} for the subject ship when fitted with single-rudder is about 0.32. For the subject ship fitted with a twin-rudder system, the w_{P0} estimated from the experiment when extrapolated to full scale is 0.336 and 0.341, corresponding to the self- propulsion point $J_S = 0.474$ and 0.484, respectively. Therefore, it can be concluded that the influence of rudder type on w_{P0} is not significant.

4.2 Effective propeller wake fraction in a maneuvering condition

To estimate w_p during a ship's maneuvering motions, captive model tests were conducted with the ship model in drift condition and the calculated variation of $(1 - w_P) - (1 - w_{P0})$ is shown in Fig. 4. The variation is similar to that of single-rudder system [13]; however, it is distinct from that of the twin-propeller twin-rudder system [4, 5]. The variation of $(1 - w_P) - (1 - w_{P0})$ for the subject ship with twin rudders using the regression form [13] $w_p = w_{p0}\exp(c_H(\beta - x'_P r')^2)$ is also shown. From experiment data, the value of the constant c_H for the subject model with twin rudders is estimated to be -3.61. A fourth-order function of v'_P as shown in Eq. 6 is found to be suitable for formulating the variation of effective wake fraction in drift condition. Although during the experiments the ship's yaw rate r is zero, the inflow to the propeller in the sway direction during maneuvering motions can be formulated with v'_P as shown in Eq. 6. The coefficient x'_P as defined for single-rudder system is also used for the twin-rudder model. This is because both the models have a single propeller, and the influence of rudder type on this coefficient is not expected to be significant for a ship's forward motion.

$$\left.\begin{aligned} 1 - w_P &= (1 - w_{P0}) + b_1\left(b_2 v'_P + \left(v'_P + b_3 v'_P|v'_P|\right)^2\right) \\ v'_P &= v' - x'_P r' \end{aligned}\right\} \tag{6}$$

4.3 Thrust deduction factor in straight running

It is common to estimate t_{P0} using Eq. 7 for model's straight running condition. The hull force X_M and propeller thrust T_M are measured during self-propulsion experiments, while the hull resistance $R(u)$ is estimated from model resistance tests. The values of t_{P0} calculated from experiment is shown in Fig. 5.

$$t_{P0} = 1 - (R(u) + X_M)/T_M \tag{7}$$

A quadratic function of J as shown in Eq. 8 is found to be suitable for formulating t_{P0}.

$$1 - t_{P0} = c_1 + c_2 J + c_3 J^2 \tag{8}$$

The values of t_{P0} estimated from Holtrop [14] for the subject ship type when fitted with a single rudder is 0.21. For the subject ship fitted with a twin-rudder system, the values of t_{P0} estimated from the experiment is 0.254 and 0.257 corresponding to the self-propulsion point $J = 0.281$ and 0.288, respectively. The full sale powering performance prediction is sensitive to the value of t_{P0} and the difference

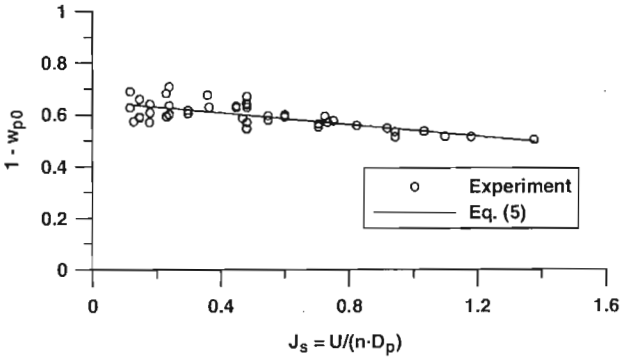

Fig. 3 Variation of $1 - w_{p0}$ for a twin rudder

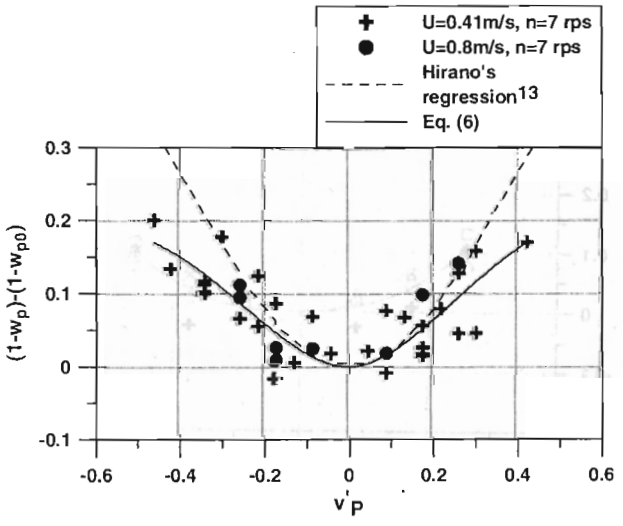

Fig. 4 Variation of $1 - w_p$ for a twin-rudder system

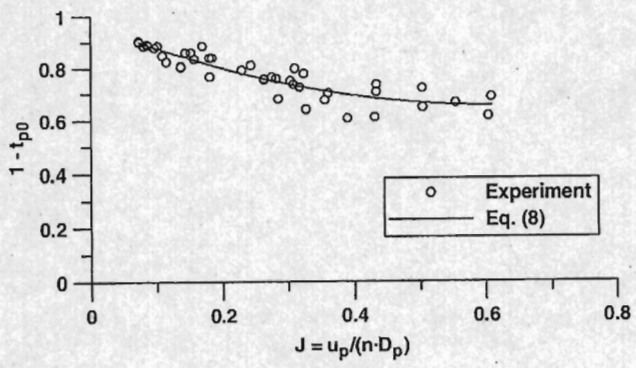

Fig. 5 Variation of $1 - t_{P0}$ for a twin-rudder system

in t_{P0} for a twin-rudder and a single-rudder system appears to be significant. This phenomenon is further discussed with other experiment results in Sect. 7.

4.4 Thrust deduction factor in a maneuvering condition

It is common to estimate t_P using Eq. 9 for model's maneuvering motions. Here, X_H is the surge direction force during ship's maneuvering motions. The variation of $(1 - t_P) - (1 - t_{P0})$ is shown in Fig. 6.

$$t_P = 1 - (X_H + X_M)/T_M \tag{9}$$

It is known that t_P for ships fitted with a single-rudder system does not vary significantly with ship's maneuvering motion; however, for a twin-rudder system the variation of t_P appears to be significant. This phenomenon has not been reported until now and needs to be confirmed for other ship types before any firm conclusions can be drawn. Although during the experiments the ship's yaw rate is zero, the inflow to propeller in sway direction during maneuvering

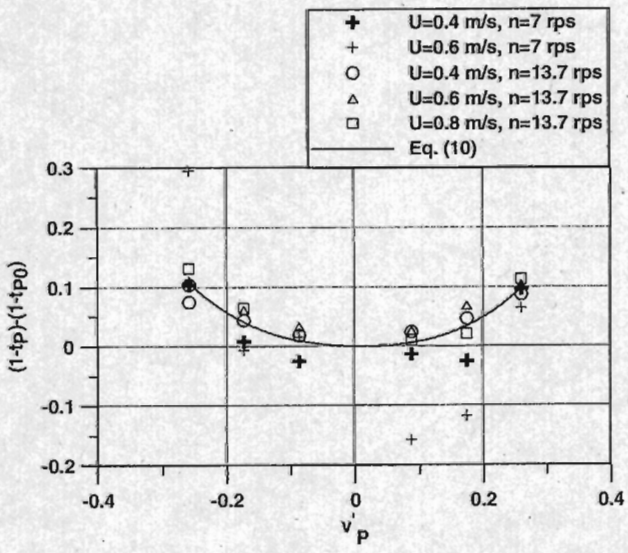

Fig. 6 Variation of $1 - t_P$ for a twin-rudder system

motions can be formulated with v_P' as shown in Eq. 10. Here, the form of regression function for $1 - t_P$ is assumed to be similar to that of $1 - w_P$.

$$1 - t_P = (1 - t_{P0}) + d_1\left(d_2 v_P' + \left(v_P' + d_3 v_P'\left|v_P'\right|\right)^2\right) \tag{10}$$

5 Mathematical model of a twin-rudder system

The MMG expression for hydrodynamic forces and moment acting on the ship due to a single rudder is modified for the twin rudders and shown in Eqs. 11–13. The sum of the force generated by each one of the twin rudders is considered as a single force, and the interactions between the hull and the twin rudders are described with a set of coefficients. To distinguish between the coefficient of starboard and port twin rudders, the subscript '*P*' and '*S*' is used in the parenthesis '{}'. When referring to the corresponding coefficient of a single rudder, these subscripts are not used. In Eq. 12, either the top line or the bottom line in the parenthesis make an equation set, combinations of top and bottom line should not be considered. This format of writing the equations will be followed in the remaining part of the paper.

$$\left.\begin{aligned} X_R &= -(1 - t_R)(F_{NS}\sin\delta_S + F_{NP}\sin\delta_P) \\ Y_R &= -(1 + a_H)(F_{NS}\cos\delta_S + F_{NP}\cos\delta_P) \\ N_R &= -(x_R + a_H x_H)(F_{NS}\cos\delta_S + F_{NP}\cos\delta_P) \end{aligned}\right\} \tag{11}$$

$$F_{N\{{}^{S}_{P}\}} = \frac{1}{2}\rho A_{R\{{}^{S}_{P}\}} F'_{N\{{}^{S}_{P}\}}\left(\alpha_{R\{{}^{S}_{P}\}}\right) U^2_{R\{{}^{S}_{P}\}} \tag{12}$$

$$\left.\begin{aligned} \alpha_{R\{{}^{S}_{P}\}} &= \delta_{\{{}^{S}_{P}\}} - \delta_{\{{}^{S}_{P}\}0} - \tan^{-1}\left(v_{R\{{}^{S}_{P}\}}/u_{R\{{}^{S}_{P}\}}\right) \\ U_{R\{{}^{S}_{P}\}} &= \sqrt{u^2_{R\{{}^{S}_{P}\}} + v^2_{R\{{}^{S}_{P}\}}} \end{aligned}\right\} \tag{13}$$

5.1 Interaction between ship and rudder

The summary of experiments carried out to determine the interaction of the ship and the twin-rudder system is shown in Table 3. The estimated values of $1 - t_R$, a_H and x'_H are shown in Fig. 7. For mariner rudder, previous studies have concluded that a_H can be expressed as a quadratic function of J [11]. For a twin-rudder system, a quadratic function of J for expressing $1 - t_R$, a_H and x'_H is used as shown in Eqs. 14, 15 and 16, respectively.

$$t_R = e_1 + e_2 J + e_3 J^2 \tag{14}$$

$$a_H = f_1 + f_2 J + f_3 J^2 \tag{15}$$

$$x'_H = g_1 + g_2 J + g_3 J^2 \tag{16}$$

The coefficient $1 - t_R$ for a twin-rudder system does not vary significantly with J and the regression coefficients e_2, and e_2 are estimated to be zero. For the subject model ship

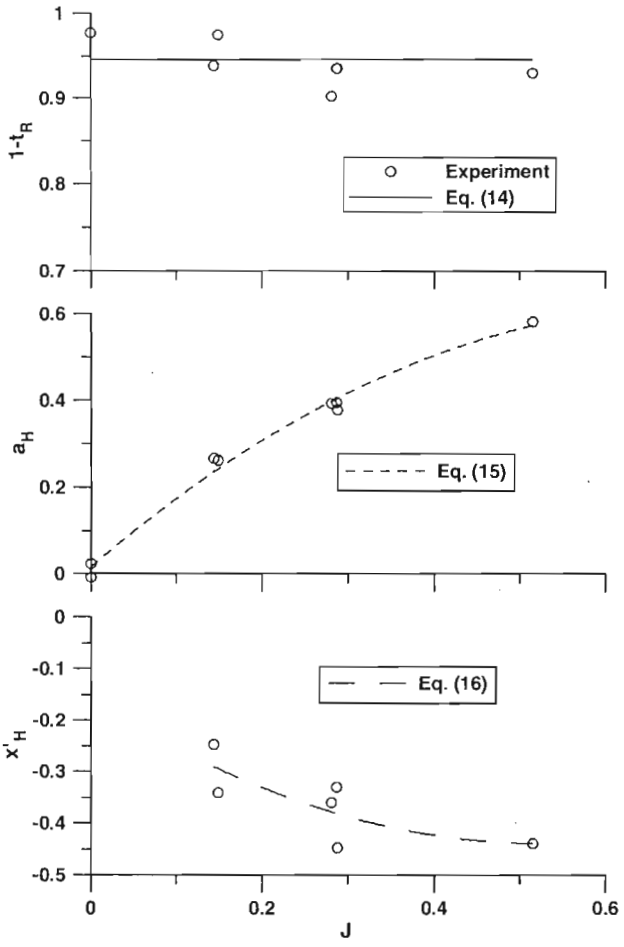

Fig. 7 Variation of $1 - t_R$, a_H and x'_H for a twin-rudder system

when fitted with a twin-rudder system, at the self-propulsion point $J = (0.281, 0.288)$ the values of $1 - t_R$, a_H and x'_H are expected to be (0.940, 0.940), (0.398, 0.405) and (−0.378, −0.381), respectively.

Hasegawa [15] showed that $1 - t_R$ for a VLCC tanker, $C_b = 0.827$, fitted with a single rudder is about 0.70. Kobayashi et al. [11] plotted $1 - t_R$, a_H and x'_H against C_b for different ship types and drew regression curves. From these regression curves the values of $1 - t_R$, a_H and x'_H are expected to be 0.778, 0.6 and −0.45, respectively, for the subject model ship when fitted with a single-rudder system. For a twin-rudder system, the values of t_R, a_H and $|x'_H|$ is lower. This is because as the rudder moves away from the hull/ship centerline, their mutual interactions are expected to reduce.

5.2 Rudder normal force

To measure non-dimensional rudder normal forces $F'_{N\{S\}_{\{P\}}}$ shown in Eq. 12, rudder open water tests were carried out in a circulating water channel at water inflow speed of 0.8 m/s. Since each, one of the twin rudders has the same cross section, only the starboard twin rudder is tested. The result of the rudder open water test is shown in Fig. 8 as symbol. The rudder is tested in steady inflow condition; therefore stall points appear below ±30° rudder angles. However, the commencement of the stall will be delayed when the rudder is operating behind the propeller. Kose et al. [16] determined the stall angle for the Schilling rudder operating behind the propeller as ±37°. The same value of the stall angle is considered for the twin-rudder system, because the cross section of each one of the twin rudders is similar to that of the Schilling rudder.

The method of predicting rudder normal force for the twin-rudder system when operating behind the propeller will be described. From rudder open water tests, $C_{N\{S\}_{\{P\}}}$ is measured. Behind propeller, the rudder normal force coefficient is calculated by $C_{N\{S\}_{\{P\}}} \sin\left(\alpha_{R\{S\}_{\{P\}}}\right)$ until the stall point $\left(\left|\delta_{\{S\}_{\{P\}}}\right| \leq \pm 37°\right)$. Here the influence of propeller rotation and ship's hull is not considered; therefore $\alpha_{R\{S\}_{\{P\}}} = \delta_{\{S\}_{\{P\}}}$. After the stall point, the measured rudder normal forces from open water experiment are non-dimensionalized and shifted up proportionately to maintain continuity of the rudder normal force coefficient at the stall point (±37°). The predicted non-dimensionalized rudder normal force is shown by hard line in Fig. 8, and it will hereafter be referred to as $F'_{N\{S\}_{\{P\}}}$ in this paper.

5.3 Rudder inflow velocity without propeller

To get rudder inflow velocity behind the ship without propeller, experiments were carried out by removing the propeller and fitting the shaft end with a fair water cap. To remove the mutual interaction between twin rudders only one of the twin rudders should be fitted, here the port twin rudder is fitted. The rudder normal force measured during the experiment is defined as F_{NPM}. During experiment

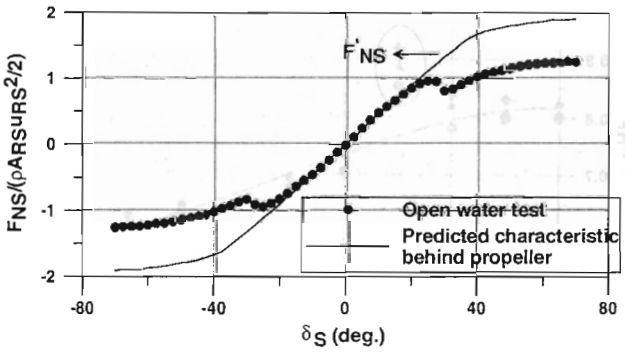

Fig. 8 Normal force characteristics of a twin-rudder system

$\beta = 0°$ and there is no influence of propeller rotation; therefore α_{RP} and U_{RP} become δ_P and u_{RP}, respectively. The nondimensional rudder normal force F'_{NP} can be determined using the rudder open water test results, since δ_P is known during experiment. Since the average flow over rudder u_{RP} is measured from the experiment data therefore, it is represented as u_{RPM}. Using Eq. 17, one can calculate w_{RP}. The values are shown in Fig. 9.

$$\left.\begin{aligned} u_{RPM} &= \sqrt{F_{NPM}/(\rho A_{RP} F'_{NP}/2)} \\ w_{RP} &= 1 - u_{RPM}/u \end{aligned}\right\} \quad (17)$$

For a single rudder the variation of w_R is symmetric on the rudder's port and starboard side. However, the characteristics of w_{RP} for a twin-rudder system are different from those of a single-rudder system. The port twin rudder moves away from the hull for tail outboard angle, understandably w_{RP} reduces; however, it does not become zero. This is because only the aft part of rudder moves away from hull, while the forward part of the rudder moves towards the hull, and overall some part of the rudder remains in the wake even at tail outboard angle. The reduction in wake at locations away from ship centerline at rudder positions have been reported earlier [17].

Due to the stall effect, sharp jump in w_{RP} value is observed at ±30° rudder angle (marked with circle in Fig. 9). The coefficient w_{RP} was formulated as function of δ_P by ignoring the value corresponding to ±30° rudder angle. A cubic function of rudder angle as shown in Eq. 18 is found to be suitable for formulating the effective wake fraction in way of the twin rudder. Without the propeller, the geometrical aspect of the starboard twin rudder is symmetrical to the port twin rudder, so w_{RS} can be formulated with this consideration.

$$1 - w_{R\{P\}^S} = a_{\{P\}^S 1} + a_{\{P\}^S 2}\delta_P + a_{\{P\}^S 3}\delta_P^2 + a_{\{P\}^S 4}\delta_P^3 \quad (18)$$

5.4 Rudder inflow velocity with propeller

For the subject twin-rudder system, the operating limits are $-30° \le \delta_S \le 60°$ and $-60° \le \delta_p \le 30°$, respectively. Considering normal rudder operating conditions, only cases where both the rudder rotate in same direction, for example, the positive starboard rudder angle with the positive port side rudder angle, were considered for experiments. During the experiments unsymmetrical rudder angles were used, so that the developed mathematical model can be used for simulating different operating conditions of the twin-rudder system. During the experiments model speed is varied while the propeller revolution is kept constant at 7 RPS.

The MMG expression for rudder inflow velocity due to the propeller for single rudder is modified for a twin-rudder system and is shown in Eq. 19. The equation can be simplified, for the case when the ship speed is zero i.e. $U = 0$ as shown in Eq. 20. For a single-rudder system, the value of k_x in Eq. 19 is determined as 0.6 [18], the same value is assumed for a twin-rudder system since both rudder systems have a single propeller.

$$\left.\begin{aligned} u_{R\{P\}^P} &= \varepsilon_{\{P\}^S} u_P \sqrt{\eta\left[1+\kappa_{\{P\}^S}\left(\sqrt{1+\frac{8K_T}{\pi J^2}}-1\right)\right]^2+(1-\eta)} \\ \varepsilon_{\{P\}^S} &= (1-w_{R\{P\}^S})/(1-w_P), \kappa_{\{P\}^S} = k_x/\varepsilon_{\{P\}^S}, \eta = D_P/h_R \end{aligned}\right\} \quad (19)$$

$$u_{R\{P\}^P} = k_x\sqrt{\frac{8C_1\eta}{\pi}}nD_P, \quad \text{at} \quad u = 0 \quad (20)$$

The rudder normal force measured during experiment $F_{N\{P\}^S M}$ is non-dimensionalized as shown in Eq. 21, and is shown as symbol in Fig. 10.

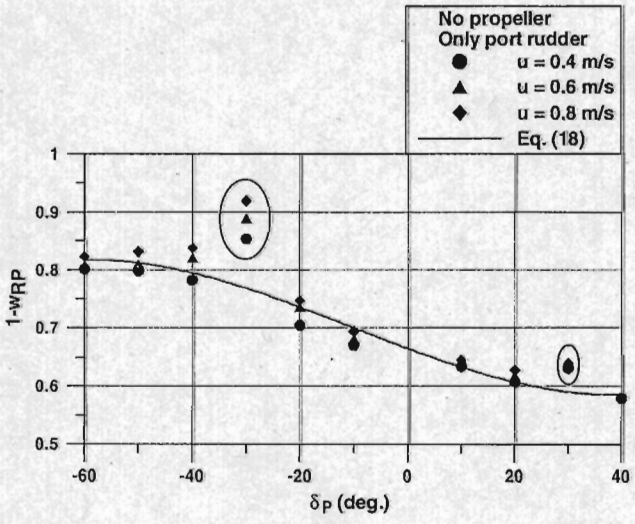

Fig. 9 Variation of $1 - w_{RP}$ for a twin-rudder system

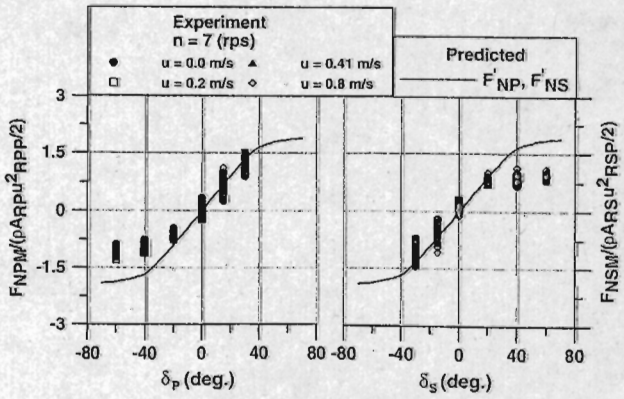

Fig. 10 Variation of nondimensional normal force

$$F'_{N\{^{S}_{P}\}M} = \frac{F_{N\{^{S}_{P}\}M}}{\left(\frac{1}{2}\rho A_{R\{^{S}_{P}\}} u^2_{R\{^{S}_{P}\}P}\right)} \quad (21)$$

During experiment $\beta = 0°$ and by ignoring the influence of propeller rotation $\delta_{\{^{S}_{P}\}0}$, $\alpha_{R\{^{S}_{P}\}} = \delta_{\{^{S}_{P}\}}$. The solid line in Fig. 10 is the $F'_{N\{^{S}_{P}\}}$ as shown in Fig. 8. The analysis of experiment data can express the variation of rudder normal force to some extent. The rudder normal force is unsymmetrical for the tail-inboard and tail-outboard condition, even though each one of the twin rudders has a symmetrical cross section about its chord line. This is because, since each one of the twin rudders is offset from the ship's longitudinal center plane, the flow velocity to each twin rudder is not symmetric as shown in Fig. 11. Therefore, although the expression in Eq. 19 is sufficient to obtain the actual rudder inflow velocity u_R for a single rudder, it cannot be directly used for a twin rudder. Similarly, the influence of $\delta_{\{^{S}_{P}\}0}$ cannot be ignored and mutual interactions between twin rudders need to be investigated; therefore, the experiment data are further analyzed for this purpose.

5.4.1 *Inflow angle to a twin-rudder system*

It is known that the angle of the propeller slip stream to the single-rudder has a significant value. In the twin-rudder system, the flow speed between the twin rudder and outside of the twin rudder is different. A sketch of the inflow to the twin rudder is shown in Fig. 11. The flow stream (B) which is directly accelerated by the propeller should be faster than the flow streams (A) and (C). Because of the above reason, the inflow angle to each one of the twin rudders is different.

To figure out the inflow angles to the twin rudders at the various conditions, two different analyses were carried out. In the first analysis, the measured rudder normal forces $F_{N\{^{S}_{P}\}M}$ when each one of the twin rudders has a zero angle, were non-dimensionalized with the calculated inflow velocity by using Eqs. 19, 20. With the non-dimensionalized rudder normal force as input data, the inflow angle to the twin-rudder system is read off from Fig. 8. The experiments that are shown in Table 3 are used for this analysis. It is assumed that the interaction between the twin rudders is small when each one of the twin rudders has zero angle, and so it is ignored in this analysis.

The example of the second analysis for the inflow angle to a twin rudder is shown in Fig. 12. The measured rudder normal forces are curve fitted with rudder angles, and the rudder angle that has zero rudder normal force, $\delta_{\{^{S}_{P}\}0}$, is read from the curve. Two different sets of the experiment were used for this analysis. In one set, the experiment was carried out with only one of the twin rudders fitted behind the propeller, while in the second set the experiment was carried out with both the twin rudders fitted behind the propeller. Additionally, in the second set of experiments when both the twin rudders are fitted behind the propeller, one of the twin rudders is kept at zero angle. The above analysis method was carried out for both port and starboard twin rudders, respectively.

The results of the analyses are shown in Fig. 13, where the rudder angle $\delta_{\{^{S}_{P}\}0}$ is plotted against propeller slip ratio s, where $s = 1 - \frac{u_P}{nP}$. A linear function of slip ratio s as shown in Eq. 22 is found to be suitable for formulating the tail inboard angle $\delta_{\{^{S}_{P}\}0}$ of the twin rudders. The model self-propulsion point is at $s = 0.57$. The values of $\left|\delta_{\{^{S}_{P}\}0}\right|$ are more than 3° at the self-propulsion point. The angles $\left|\delta_{\{^{S}_{P}\}0}\right|$ are further increased when the ship's speed is reduced with the same RPS in the acceleration conditions. With these results, it can be concluded that $\left|\delta_{\{^{S}_{P}\}0}\right|$ increases when the ratio of the flow speed (B) and the flow speeds (A) (C) increases. Different behavior was observed during the experiment at zero ship speed, when $s = 1$. The angles $\delta_{\{^{S}_{P}\}0}$ at these conditions are smaller than the values expressed with the Eq. 22.

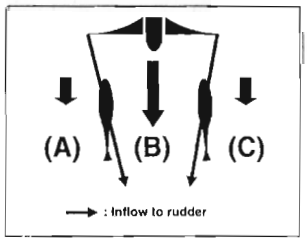

Fig. 11 Sketch of inflow to a twin-rudder system

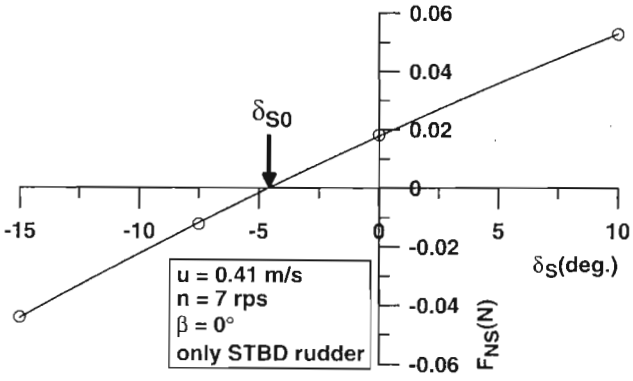

Fig. 12 Example of analysis for inflow angle to the twin rudders

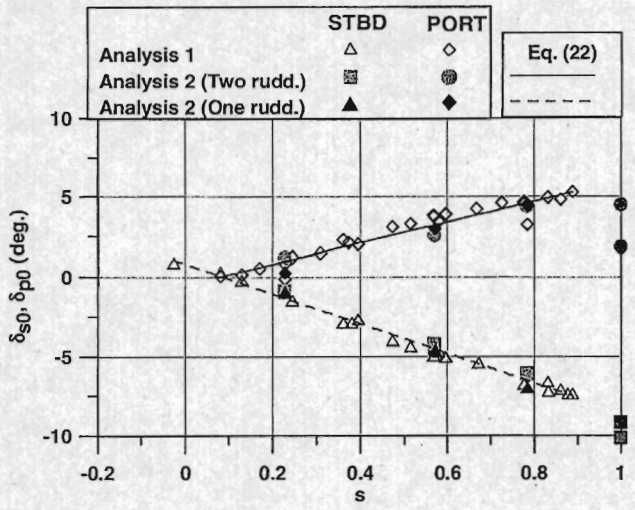

Fig. 13 Variation of $\delta_{\{S\}_0}$ for a twin-rudder system

$$\left.\begin{aligned}\delta_{\{S\}_0} &= b_{\{S\}_1} + b_{\{S\}_2} s \\ \delta_{\{S\}_1} &= \delta_S - \delta_{\{S\}_0}\end{aligned}\right\} \tag{22}$$

It is considered that when the ship is not moving, the flow stream (B) in Fig. 11 is much more accelerated by the propeller rotation. In the subsequent analysis for zero ship speed, $\delta_{\{S\}_0}$ obtained from analysis 2 is used to analyze the interaction between the twin rudders. However, the zero ship speed in real operation happens only for an instant, so this phenomenon was not considered for modeling the twin rudders.

5.4.2 *Interaction between twin rudders*

The interaction between twin rudders can be gauged from Fig. 11. The flow stream (B) is deflected when either one of the twin rudders has certain rudder angle. The interaction between the twin rudders is analyzed as per analysis 2 described earlier. The analysis 2 was carried out when the opposite side rudder has zero angle. In this case analysis was carried out with the opposite rudder having certain angles as shown in Table 3. The measured rudder normal forces are curve fitted with rudder angles, and the angle $\delta_{\{S\}\{P\}} + \delta_{\{S\}_0}$ at which rudder normal force is zero, when the other side rudder has a certain angle is read from the curve. Using Eq. 22, one can determine $\delta_{\{S\}_0}$ since u and n are known during experiment and interaction between the twin rudders $\delta_{\{S\}\{P\}}$ is calculated. The results are shown in Fig. 14. The interaction between a twin rudder $\delta_{\{S\}\{P\}}$ is influenced both by the opposite rudder angle and slip ratio s. The interaction between the twin rudder at zero rudder angle for different slip ratios s is already formulated in Eq. 22. Therefore, $\delta_{\{S\}\{P\}}$ is considered to be zero when $\delta_{\{S\}}$ are zero. A quadratic

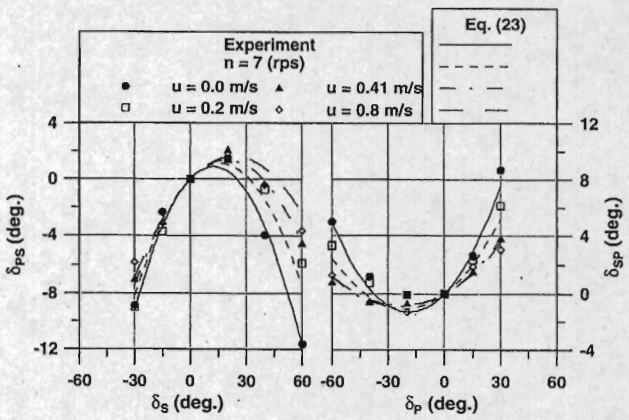

Fig. 14 Variation of $\delta_{\{S\}\{P\}}$ for a twin rudder. δ_{SP}, interaction on the starboard twin rudder due to the port twin rudder; δ_{PS}, interaction on the port twin rudder, due to the starboard twin rudder; δ_S, angle of the starboard twin rudder; δ_P, angle of the port twin rudder

function of both slip ratio s and the opposite rudder angle $\delta_{\{P\}}$, respectively, as shown in Eq. 23 is suitable for formulating the coefficient $\delta_{\{S\}\{P\}}$.

$$\left.\begin{aligned}\delta_{\{S\}\{P\}} &= c_{\{S\}_1}\delta_S^P + c_{\{S\}_2}\delta_S^{P2} \\ c_{\{S\}_1} &= d_{\{S\}_1} + d_{\{S\}_2} s + d_{\{S\}_3} s^2 \\ c_{\{S\}_2} &= e_{\{S\}_1} + e_{\{S\}_2} s + e_{\{S\}_3} s^2 \\ \delta_{\{S\}_2} &= \delta_{\{S\}_1} - \delta_{\{S\}\{P\}}\end{aligned}\right\} \tag{23}$$

where

$$\delta_{\{S\}\{P\}} = \delta_{\{S\}\{P\}} \quad \text{if} \quad \delta_{\{S\}_1} > 0$$

$$\delta_{\{S\}\{P\}} = \delta_{\{S\}\{P\}} \cos\left(\delta_{\{S\}_1}\right) \quad \text{if} \quad \delta_{\{S\}_1} > 0$$

5.4.3 *Decrement of inflow velocity to the twin rudders*

The effective rudder angle $\delta_{\{S\}_2}$ during experiment can be calculated using Eqs. 22, 23 since $\delta_{\{S\}}$, n, u, T_M and $F_{N\{S\}M}$ are known during experiment. The non-dimensional rudder normal force $F'_{N\{S\}}$ is obtained from Fig. 8 with $\delta_{\{S\}_2}$ as the input data. The actual inflow velocity to each one of the twin rudders behind the ship and propeller is defined as $u_{R\{S\}M}$ and can be calculated by using Eq. 24. For a twin-rudder system, the inflow velocity $u_{R\{S\}M}$ and $u_{R\{S\}P}$ are similar for the tail inboard angle; however, they are different for the tail outboard angle. Therefore, decrement of inflow velocity at tail outboard condition $f_{R\{S\}}$ for twin rudders can be defined as shown in Eq. 25.

$$u_{R\{P\}M} = \sqrt{\frac{F_{N\{P\}M}}{\left(\frac{1}{2}\rho A_{R\{P\}} F'_{N\{P\}}\right)}} \tag{24}$$

$$f_{R\{P\}} = u_{R\{P\}M} / u_{R\{P\}P} \tag{25}$$

The decrement ratio $f_{R\{P\}}$ calculated from the experiment data by Eqs. 24, 25 is shown in Fig. 15. The decrement ratio $f_{R\{P\}}$ at the tail outboard condition corresponds to the effective rudder angle $\delta_{\{P\}2}$ and s. A quadratic function of both $\delta_{\{P\}2}$ and s respectively as shown in Eq. 26 is suitable for formulating the decrement ratio $f_{R\{P\}}$ of twin rudders. The actual inflow velocity to the twin rudders $u_{R\{P\}}$ in surge direction is formulated as shown in Eq. 27.

$$\left.\begin{aligned} f_{R\{P\}} &= f_{\{P\}1} + f_{\{P\}2}\delta_{\{P\}2} + f_{\{P\}3}\delta^2_{\{P\}2} \\ f_{\{P\}1} &= g_{\{P\}1} + g_{\{P\}2}s + g_{\{P\}3}s^2 \\ f_{\{P\}2} &= h_{\{P\}1} + h_{\{P\}2}s + h_{\{P\}3}s^2 \\ f_{\{P\}3} &= k_{\{P\}1} + k_{\{P\}2}s + k_{\{P\}3}s^2 \end{aligned}\right\} \tag{26}$$

$$u_{R\{P\}} = f_{R\{P\}} \cdot u_{R\{P\}P} \tag{27}$$

The decrease in rudder normal force due to the stall can occur at large rudder angles and the rudder normal forces are predicted considering stall angle [16]. The effect of the stall may, therefore, be included in the decrement of inflow velocity to the twin rudders with this analysis.

The non-dimensional rudder normal forces after considering the hull-rudder interactions and mutual interactions of the twin rudder are shown in Fig. 16 and the analyzed experiment data have good agreement with the predicted rudder normal force.

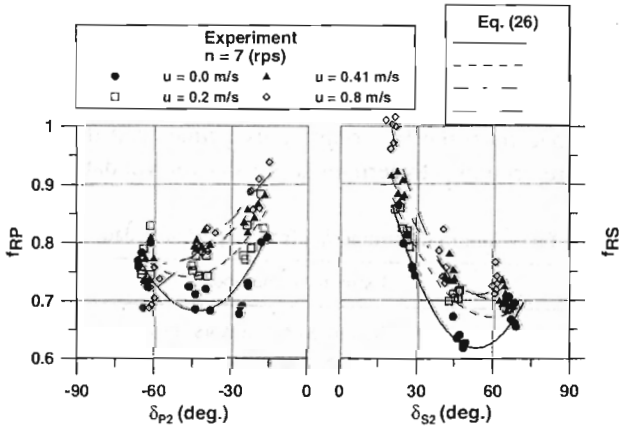

Fig. 15 Variation of $f_{R\{P\}}$ for twin rudders. f_{RP}, decrement of inflow velocity for the port twin rudder; f_{RS}, decrement of inflow velocity for the starboard twin rudder; δ_{P2}, effective inflow angle of the port twin rudder; δ_{S2}, effective inflow angle of the starboard twin rudder

5.4.4 *Influence of ship's maneuvering motion on flow straightening coefficient of twin rudders*

The variation of inflow rudder angle due to ship's motion can be expressed with Eqs. 28 and 29 for a twin-rudder system.

$$v_{R\{P\}} = -\gamma_{R\{P\}} v - l_{R\{P\}} r \tag{28}$$

$$\alpha_{R\{P\}} = \delta_{\{P\}2} - \tan^{-1}\left(v_{R\{P\}}/u_{R\{P\}}\right) \tag{29}$$

The effect of ship's sway and yaw motion has been formulated separately unlike in the case of a single rudder. This is because it is expected that the influence of these motions may be different for a twin rudder. For example, the variation of inflow to a port twin rudder due to ship's sway and yaw motion may not be same due to the presence of a starboard twin rudder. The experiments to figure out the effect of the sway motion were carried out at different drift angles with zero yaw rate. The rudder angle combinations for the experiments were selected as explained in Sect. 5.4. The expression for rudder normal force shown in Eq. 12 can be written as shown in Eq. 30.

$$\begin{aligned} F_{N\{P\}M} = {} & \frac{1}{2}\rho A_{R\{P\}} C_{N\{P\}} \\ & \times \sin\left(\delta_{\{P\}2} - \tan^{-1}\left(\frac{-\left(\gamma_{R\{P\}}\right)v}{u_{R\{P\}}}\right)\right) \\ & \times \left(u^2_{R\{P\}} + \left(-\gamma_{R\{P\}} v\right)^2\right) \end{aligned} \tag{30}$$

The procedure for determining $\gamma_{R\{P\}}$ from Eq. 30 is described in Table 4 and its calculated values are shown in Fig. 17. The flow straightening coefficients $\gamma_{R\{P\}}$ vary both with the effective rudder angles and β. A quadratic function

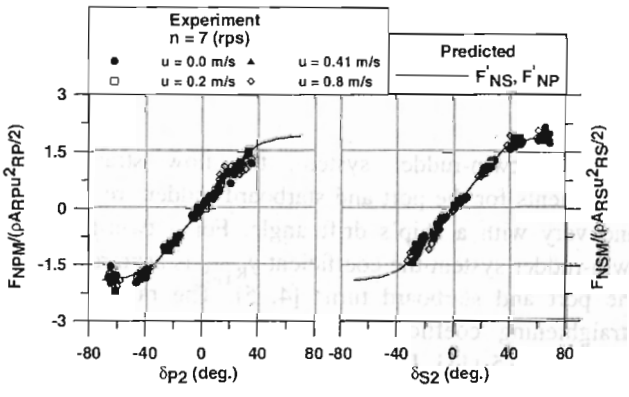

Fig. 16 Variation of nondimensional normal force for twin rudders after considering all interactions

Table 4 Procedure to determine $\gamma_{R\{P\}}^{S}$ from experiment data

Parameter	Estimation method
$F_{N\{P\}M}^{S}$, u, v, n, δ_P^S	Recorded by sensors during experiment
$\delta_{\{P\}2}^{S}$	Eq. 23
$u_{R\{P\}}^{S}$	Eq. 27
ρ, $A_{R\{P\}}^{S}$	Known constants
$C_{N\{P\}}^{S}$	From rudder open water tests
$\gamma_{R\{P\}}^{S}$	Solving Eq. 30 by least square method

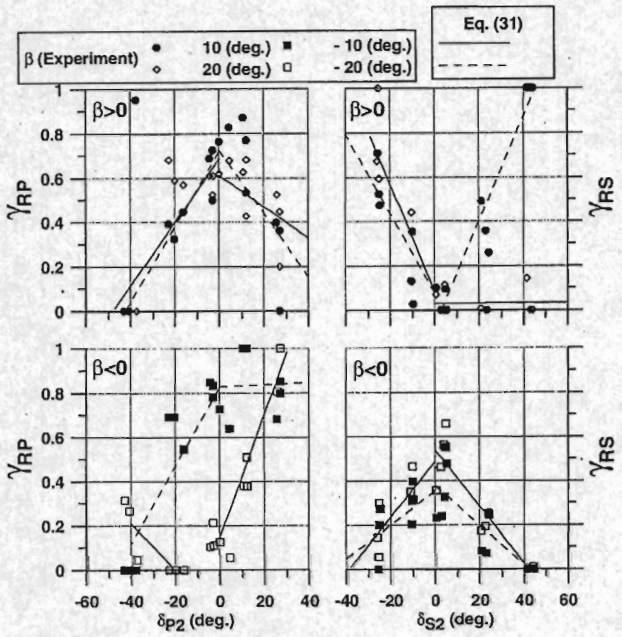

Fig. 17 Variation of γ_{RS} and γ_{RP} for a twin rudder. γ_{RS}, flow straightening coefficient for the starboard twin rudder; γ_{RP}, flow straightening coefficient for the port twin rudder; δ_{S2}, effective inflow angle of the starboard twin rudder; δ_{P2}, effective inflow angle of the port twin rudder

of drift angle β and linear function of the effective rudder inflow angle $\delta_{\{P\}2}^{S}$, respectively, as shown in Eq. 31 is suitable for formulating the coefficients $\gamma_{R\{P\}}^{S}$.

$$\gamma_{R\{P\}}^{S} = \left(r_{\{P\}1}^{S} + r_{\{P\}2}^{S}|\beta| + \left(r_{\{P\}3}^{S} + r_{\{P\}4}^{S}|\beta|\right)\delta_{\{P\}2}^{S}\right)|\beta| \tag{31}$$

For a twin-rudder system, the flow straightening coefficients for the port and starboard rudder are different and vary with a ship's drift angle. For a twin-propeller twin-rudder system the coefficient $\gamma_{R\{P\}}^{S}$ is asymmetric for the port and starboard turns [4, 5]. The range of flow straightening coefficient for a single-rudder system is $0 \le \gamma_R \le 0.5$ [11]. It must, however, be noted that $\gamma_{R\{P\}}^{S}$ for a twin-rudder system described in this paper is different from γ_R for a single-rudder system, because expression for Eq. 28 will be different for a single-rudder system.

During captive model experiments, the ship's yaw rate is kept zero; therefore, a procedure to determine $l_{R\{P\}}^{S}$ from the free running experiments is developed and explained here. Since the twin-rudder arrangement is symmetric, the coefficients $l_{R\{P\}}^{S}$ are assumed to be symmetric, here l_{RS} is determined; therefore during the experiment the sensor to measure rudder normal force is installed on the stock of starboard twin rudder. The rudder normal force measured during the free running experiments is asymmetric for the ship's starboard and port turns. This is because for starboard turns, the starboard rudder is on the leeward side, while the port rudder is on the windward side of the flow and vice-versa. Therefore, a zigzag experiment is used to determine the coefficient l_{RS}. For ease of understanding, Eq. 12 can be written as Eq. 32.

$$F_{NSM} = \left(\frac{1}{2}\rho A_{RS} C_{NS}\right)\left(u_{RS}^2 + (-\gamma_{RS} v - l_{RS} r)^2\right) \times \sin\left(\delta_{S2} - \tan^{-1}\left(\frac{(-\gamma_{RS} v - l_{RS} r)}{u_{RS}}\right)\right) \tag{32}$$

The procedure to determine l_{RS} from Eq. 32 is shown in Table 5. A nonlinear function of x_R as shown in Eq. 33 is suitable for formulating the coefficient l_{RS}. The rudder normal force measured during experiment (LHS of Eq. 32) is compared with the values estimated by the mathematical model (RHS of Eq. 32) and shown in Fig. 18. The model described in Eq. 33 represents well the experiment results.

$$l_{R\{P\}}^{S} = c_{\{P\}}^{S} x_R \tag{33}$$

6 Validation of mathematical model of twin rudders with free running experiments

The model ship used for developing the mathematical model of the single-propeller twin-rudder ship was also used for the simulations and the free running experiments. Simulations and free running experiment were carried out at cruising speed, which is 0.8 m/s for the model ship and 13.5 knots for a full-scale ship. Since the coefficient l_{RS} is determined from the free running experiments, a different set of free running experiments is used for validating the

Table 5 Procedure to determine l_{RS} from experiment data

Parameter	Estimation method
F_{NSM}, u, v, r, n, δ_P^S	Recorded by sensors during experiment
δ_{S2}	Eq. 23
u_{RS}	Eq. 27
γ_{RS}	Eq. 31
ρ, A_{RS}	Known constants
C_{NS}	Rudder open water tests
l_{RS}	Solving Eq. 32 by numerical simulations

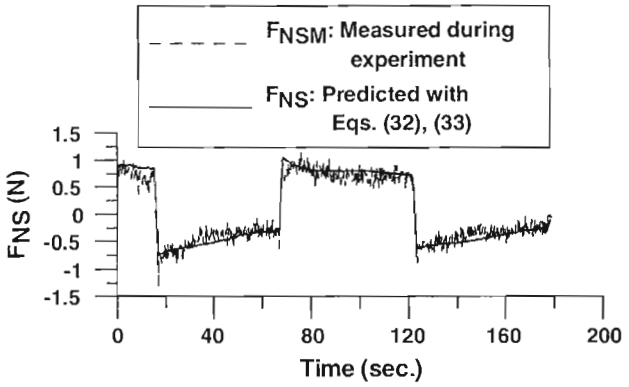

Fig. 18 Comparison of measured and predicted normal force for starboard twin rudder during zigzag test

model. Figure 19 shows trajectory of ship and the time histories of velocity parameters at $\delta_{S_P} = -30°$ turning test. The hydrodynamic hull forces and moment during simulations is predicted by Kang's model [19]. It may be noted that trajectory of the simulation is slightly deviated from that of the experiment; however, the time histories of forward velocity, lateral velocity and yaw rate matches well with that of experiment. Figure 20 shows time histories of yaw angles, rudder angles and the time histories of velocity parameters at 20/20 zigzag test. The result of the simulation shows small deviation from experiment at first overshoot angle, but has good agreement with rest of the experiment data. From the above results, it can be concluded that the developed model is suitable for expressing the motion of the ship installed with single-propeller twin-rudder system.

7 Discussion

The characteristics of a twin-rudder system are observed to be distinct from both a single-rudder system and a twin-propeller twin-rudder system. In the twin-propeller twin-rudder [4, 5] system, the unique characteristics are the asymmetric behavior of the propeller-effective wake and the flow straightening factor during ship's maneuvering motion. In the twin-rudder system, the distance between the twin rudders is less and each rudder's movement influences the other rudder's performance, additionally each one of the twin rudders is not in the longitudinal center plane of the propeller slipstream; thus the effective wake fraction, the rudder inflow velocity and flow straightening factor for the twin-rudder system are observed to be asymmetric in maneuvering motion. The mathematical model for the twin-rudder system is developed through experiments with a VLCC model. It is necessary to investigate the suitability of the mathematical model for other ship types, especially those with fine hull forms like container ships, PCCs, etc. In this study, a method of determining the coefficients that depend on the yaw rate from the free running tests is proposed due to the restriction of the captive model testing facility. It is possible to determine all the coefficients of the proposed mathematical model precisely by rotative captive model tests. The other aspect to be considered is the propulsion performance of the twin-rudder system. As explained in Sect. 2, a twin-rudder system has higher normal force characteristics as compared to mariner rudder; therefore, the drag characteristics of twin rudders will also be different as compared to the mariner rudder. Additionally in the twin-rudder system, since each one of the twin

Fig. 19 Turning test with cruising speed

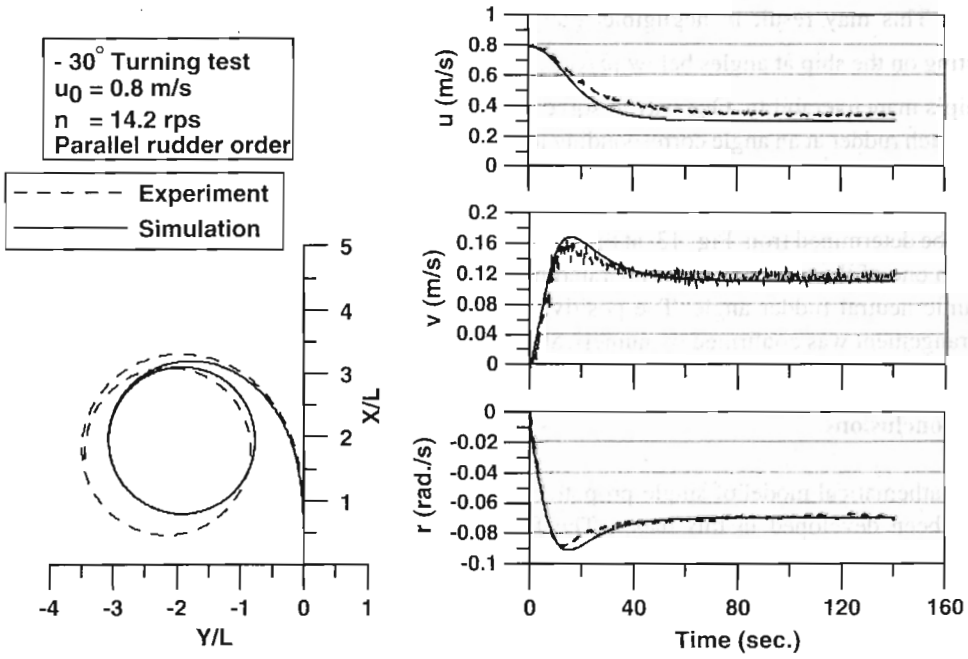

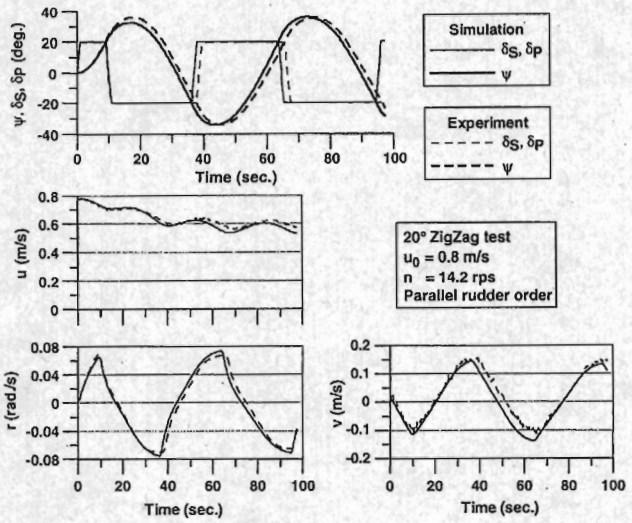

Fig. 20 Zigzag test with cruising speed

rudders is not at the longitudinal center plane of propeller slipstream, the flow characteristics of twin rudders is different from those of a single rudder as shown in Sect. 5.4. These factors will influence the scaling up of both the twin-rudder drag as well as propulsion coefficients like t_{P0}, w_{P0}, η_R etc. and further investigations are necessary.

In Sect. 5.4, it is shown that the inflow angle to each one of the twin rudders is not parallel to the longitudinal direction of the ship. It is also shown that the magnitudes of the effective inflow angles are different for the port and starboard twin rudders, and they vary with the propeller slip ratio. Due to this reason, if the twin rudder is installed by aligning each one of the twin rudders with the longitudinal direction of the ship, then at angles below $\left|\delta_{\{P\}0}\right|$, the lift force from each one of the twin rudders may act in the opposite direction on the hull. This may result in negligible total rudder lift force acting on the ship at angles below $\left|\delta_{\{P\}0}\right|$, thereby reducing ship's maneuverability. One way to solve this problem is to set each rudder at an angle corresponding to the inflow angle to the rudder, which is hydrodynamic neutral rudder angle or virtual zero rudder angle. For the subject model, this angle can be determined from Fig. 13, at the self-propulsion point. Each one of the twin rudders is operated from the hydrodynamic neutral rudder angle. The positive influence of this arrangement was confirmed by numerical simulations [20].

8 Conclusions

A mathematical model of single-propeller twin-rudder ship has been developed in this paper. The following are the main conclusions of this paper:

1. A mathematical model of single-propeller twin-rudder ship, compatible with MMG model, suitable for large vessels has been developed, based on the rudder forces and interactions among the hull, propeller and the twin rudders that are determined from model experiments.
2. Factors affecting the performance of the twin rudders have been identified. These are the inflow angle to each of the twin rudders, interactions between the twin rudders and decrement of inflow velocity to the twin rudders. A method of incorporating these factors in the mathematical model has been presented.
3. The interactions between the hull, propeller and twin rudders, including interactions between the twin rudders, were analyzed based on experiment data. Some of the interaction coefficients of the twin rudders, especially $1-t_R$, a_H, x'_H and $\gamma_{R\{P\}}$ were compared with published values of mariner rudder. Variation in some of these interaction coefficients with respect to the mariner rudder was observed and further investigations are necessary.
4. Form and variables of regression model derived for estimating various coefficients of the mathematical models of twin rudders have been identified. Regression formulas for some of the interaction coefficients were observed to be similar to that of mariner rudder. Regression formulas for some of the interaction coefficients, which are unique for a twin-rudder system, have also been derived and explained. The mathematical model of the twin-rudder system is validated based on the free running tests with VLCC model ship. It is observed that the model simulated well the free running experiments.
5. It is observed that the twin-rudder system may be installed with tail inboard angle.

Acknowledgments Japan Hamworthy Co. Ltd. has initiated this research and offered the authors an opportunity to take part in and provide the maximum convenience. The authors would like to show their gratitude for their collaboration and contribution.

Appendix

The numerical values of regression coefficients of different regression functions shown in the paper are presented in this appendix. In the figures, for ease of understanding, all the angles have been shown as degrees. However, all the regression coefficients presented here were estimated considering angles in radians (Tables 6, 7, 8, 9, 10 and 11).

Table 6 Hull and propeller interaction coefficients

$1-w_{P0}$	a_1	0.652	a_2	−0.112	a_3	0
$1-t_{P0}$	c_1	0.972	c_2	−1.04	c_3	0.845
$1-w_P$	b_1	2.227	b_2	0.006	b_3	−0.85
$1-t_P$	d_1	0.776	d_2	−0.024	d_3	1.558
x'_P	−0.50					

Table 7 Hull and twin-rudder interaction coefficients

t_R	e_1	0.06	e_2		0	e_3		0	
a_H	f_1	0.016	f_2		1.69	f_3		−1.179	
x'_H	g_1	−0.159	g_2		−1.065	g_3		1.01	
$1 - w_{RS}$	a_{S1}	0.665	a_{S2}	0.19		a_{S3}	0.051	a_{S4}	−0.095
$1 - w_{RP}$	a_{P1}	0.665	a_{P2}	−0.19		a_{P3}	0.051	a_{P4}	0.095
δ_{S0}	b_{S1}		0.015			b_{S2}		−0.164	
δ_{P0}	b_{P1}		−0.008			b_{P2}		0.114	

Table 8 Mutual interaction between twinrudders

δ_{SP}	d_{S1}	0.129	d_{S2}	−0.259	d_{S3}	0.343
	e_{S1}	0.088	e_{S2}	−0.11	e_{S3}	0.162
δ_{PS}	d_{P1}	−0.18	d_{P2}	0.085	d_{P3}	−0.226
	e_{P1}	0.14	e_{P2}	0	e_{P3}	0

Table 9 Decrement of inflow velocity to twin rudders at tail outboard rudder angle

	Condition	Coefficients						Regard
f_{RS}	$\delta_{S2} > 0$	g_{S1}	1.399	g_{S2}	−3.239	g_{S3}	2.598	$0 < f_{RS} < 1$
		h_{S1}	−2.489	h_{S2}	5.243	h_{S3}	−4.159	
		k_{S1}	1.791	k_{S2}	−1.861	k_{S3}	1.348	
	$\delta_{S2} \leq 0$	$f_{RS} = 1$						
f_{RP}	$\delta_{P2} \geq 0$	$f_{RP} = 1$						
	$\delta_{P2} < 0$	g_{P1}	0.011	g_{P2}	0.176	g_{P3}	0.38	$0 < f_{RP} < 1$
		h_{P1}	0.343	h_{P2}	−0.151	h_{P3}	0.657	
		k_{P1}	1	k_{P2}	0	k_{P3}	0	

Table 10 Effect of ship's sway motion to inflow angle of twin rudders

	Condition	Coefficients				Regard
		r_{S1}	r_{S2}	r_{S3}	r_{S4}	
γ_{RS}	$\beta \geq 0, \delta_{S2} < 0$	0.615	−1.068	−7.823	11.07	$0 \leq \gamma_{RS} \leq 0.8$
	$\beta < 0, \delta_{S2} < 0$	2.66	−3.611	2.971	−2.602	$0 \leq \gamma_{RS} \leq 0.8$
	$\beta \geq 0, \delta_{S2} \geq 0$	−0.864	2.719	15.43	−44.18	$0 \leq \gamma_{RS} \leq 0.8$
	$\beta < 0, \delta_{S2} \geq 0$	2.781	−3.55	−3.787	4.834	$0 \leq \gamma_{RS} \leq 1$
		r_{P1}	r_{P2}	r_{P3}	r_{P4}	
γ_{RP}	$\beta \geq 0, \delta_{P2} \leq 0$	6.256	−12.3	8.759	−18.38	$0 \leq \gamma_{RP} \leq 1$
	$\beta < 0, \delta_{P2} \leq 0$	10.07	−30.62	13.36	−43.29	$0 \leq \gamma_{RP} \leq 0.8$
	$\beta \geq 0, \delta_{P2} > 0$	6.559	−13.77	−8.238	20.25	$0 \leq \gamma_{RP} \leq 0.8$
	$\beta < 0, \delta_{P2} > 0$	9.064	−24.76	−4.256	25.31	$0 \leq \gamma_{RP} \leq 0.8$

Table 11 Effect of ship's yaw motion to inflow angle of twin rudders

	Condition		c_S, c_P
l_{RS}	$r \geq 0$	$\delta_{S2} \geq 0$	0
		$\delta_{S2} < 0$	0.2
	$r < 0$	$\delta_{S2} \geq 0$	0.6
		$\delta_{S2} < 0$	0.4
l_{RP}	$r \geq 0$	$\delta_{P2} \geq 0$	0.4
		$\delta_{P2} < 0$	0.6
	$r < 0$	$\delta_{P2} \geq 0$	0.2
		$\delta_{P2} < 0$	0

References

1. The Naval Architect (1985) The Royal Institution of Naval Architects, London, April issue:E185
2. Hasegawa K, Kang DH, Sano M et al (2006) Study on maneuverability of a large vessel installed with a mariner type Super VecTwin rudder. J Mar Sci Technol 11:88–99
3. MMG (1980) MMG report V (in Japanese). Bull Soc Nav Archit Jpn 616:565–576
4. Lee SK, Fujino M, Fukasawa T (1988) A study on the manoeuvring mathematical model for a twin-propeller twin-rudder ship (in Japanese). J Soc Nav Archit Jpn 163:109–118
5. Lee SK, Fujino M (2003) Assessment of a mathematical model for the manoeuvring motion of a twin-propeller twin-rudder ship. Int Shipbuild Progress 50:109–123
6. Yoshimura Y, Sakurai H (1989) Mathematical model for the manoeuvring ship motion in shallow water (3rd report)—Manoeuvrability of a twin-propeller twin-rudder ship (in Japanese). J Kansai Soc Nav Archit Jpn 211:115–126
7. Kobayashi H, Ishibashi A, Shimokawa K et al (1994) A study on Mathematical model for the maneuvering motions of twin-propeller twin-rudder ship (in Japanese). J Jpn Inst Navig 91:263–270
8. Yumuro A (1984) Some experiments on rudder force of a twin-screw ship with a single rudder (in Japanese). J Kansai Soc Nav Archit Jpn 194:53–64
9. Hamamoto M, Enomoto T (1997) Maneuvering performance of a ship with VecTwin rudder system. J Soc Nav Archit Jpn 181:197–204
10. Proceedings of 15th ITTC (1978) Appendix to the report of the performance committee of the 15th International Towing Tank Conference
11. Kobayashi E, Kagemoto H, Furukawa Y (1995) Mathematical models of maneuvering motions (in Japanese) In: Research on ship maneuverability and its application to ship design, Proceedings of the 12th marine dynamic symposium, pp 23–89
12. Lewis EV (1988) Principles of Naval Architecture second revision, vol II, SNAME, Jersey City
13. Hirano M (1980) On calculation method of ship maneuvering motion at initial design phase. J Soc Nav Archit Jpn 147:144–153
14. Holtrop J (1984) A statistical reanalysis of resistance and propulsion data, International Shipbuilding Progress, 31:272–276
15. Hasegawa K (1980) On a performance criterion for autopilot navigation. J Kansai Soc Nav Archit 178:93–104
16. Kose K, Hosokawa M, Yamada H et al (1992) A study on performance estimation of special rudders (in Japanese). Trans West Jpn Soc Nav Archit 84:49–57
17. Toda Y, Stern F, Tanaka I, Patel VC (1990) Mean-flow measurements in the boundary layer and wake of a series 60 Cb = 0.6 model ship with and without propeller. J Ship Res 34:225–252
18. Mori M (1974) Calculation of normal force of rudder behind propeller (in Japanese). J Kansai Soc Nav Archit 153:81–90
19. Kang DH, Hasegawa K (2007) Prediction method of hydrodynamic forces acting on the hull of a blunt-body ship in the even keel condition. J Mar Sci Technol 12:1–14
20. Kang DH (2006) Maneuvering mathematical model of blunt-body ship installed with mariner type VecTwin rudder. Doctoral thesis, Osaka University